Effect of symmetry breaking on bound states in the continuum in waveguide arrays

J. Petráček [1,2] and V. Kuzmiak [3,*]

[1] *Institute of Physical Engineering, Faculty of Mechanical Engineering, Brno University of Technology, Technická 2, 616 69 Brno, Czech Republic*

[2] *Central European Institute of Technology, Brno University of Technology, Purkyňova 656/123, 612 00, Brno, Czech Republic*

[3] *Institute of Photonics and Electronics, Academy of Sciences of the Czech Republic, v.v.i., Chaberská 57, 182 51, Praha 8, Czech Republic*

(Received 31 December 2021; accepted 19 May 2022; published 3 June 2022; corrected 3 August 2022)

We developed the theoretical framework based on the coupled-mode theory which describes spectral and scattering properties of the photonic analog of an extended Fano-Anderson model—a waveguide array with two additional side-coupled waveguides. The structure supports a rich spectrum of eigenmodes, including bound state in the continuum (BIC) and other bound and leaky modes, which can be classified according to the relation between the self-coupling coefficients and eigenvalues. We focus on the structures with broken vertical symmetry with their band structures revealing interesting phenomena, such as exceptional points and level repulsion, and offer a lossless platform for $\mathcal{PT}$-symmetry phase transition. We interpreted the resonant features in the scattering spectra through a generalized Weierstrass factorization. The resonance related with quasi-BIC arises from the interference between two leaky modes: one of them representing a continuum spectrum and the other (quasi-BIC) discrete state. The reflectance near the resonance can be rewritten into the form of the Fano formula where the shape parameter f can be expressed in terms of the poles associated with the two modes. Our approach provides a flexible framework which allows to interpret and to engineer the resonant properties of more complex systems.

DOI: 10.1103/PhysRevA.105.063505

I. INTRODUCTION

The bound state in the continuum (BIC) was proposed at first in quantum mechanics [1] as a special solution of the Schrödinger equation in which positive discrete energies remain localized within the continuous spectrum. The discovery has never been implemented in quantum system, however, much later the nonradiating states have been experimentally observed in electromagnetic, acoustic, and water waves [2–4]. As a general wave phenomenon, BICs arise due to several distinct mechanisms and exist in a wide range of material platforms. In this paper, we focus on so-called symmetry-protected BICs where a bound state of one symmetry class completely decouples from the continuous spectrum of another symmetry class. BICs belong to the broad group of exceptional resonant effects the origin of which can be traced back to the properties of poles and zeros of the underlying scattering matrix. Specifically, the BIC was identified as the limiting case of general Hermitian scatterer when the pole and zero of Hermitian system coalesce on the real axis with mutual coherent destruction [5].

The ideal BIC represents a resonance with zero leakage and zero linewidth, however, in practice BICs manifest themselves as "quasi-BICs" leaky modes whose Q factors are limited by material and geometrical parameters. BIC relates fundamentally to the Fano resonance which manifests itself as a sharp asymmetric profile of the transmission or the absorption lines and appears in the systems characterized by a certain discrete energy state that interacts with the continuum spectrum through an interference effect [6].

The resonant coupling and interaction between a discrete state and a continuum spectrum can occur in the so-called Fano-Anderson model [7]. The bistable wave transmission and the effect of nonlinearity on Fano resonance was described in the model that can be regarded as the nonlinear generalization of the Fano-Anderson system [8]. The formation of the surface Fano state of in a semi-infinite waveguide array with one side-coupled waveguide was observed experimentally in Ref. [9].

In this paper we employ a theoretical model described in our recent paper [10] to investigate the properties of the coupled waveguide system consisting of an infinite one-dimensional array of identical and regularly spaced single-mode optical waveguides with two additional waveguides above and below the central waveguide of the array (Fig. 1). We note that a similar structure consisting of a discrete linear chain, which in addition to Fano defects contains one δ-like defect which gives rise to the Fano-Feshbach resonance, was considered in Ref. [11]. Our model represents an extension of a photonic implementation of the Fano-Anderson model and generalization of a famous finite configuration in which an optical symmetry-protected BIC was confirmed experimentally [12]. Surprisingly, a comprehensive theoretical understanding of the system has not yet been presented.

The paper is organized as follows. In Sec. II we describe our model and systematically explore its spectral properties considering the structures with the preserved and broken vertical symmetry. In Sec. III we present the amplitude transmittance t and reflectance r of the Bloch waves and demonstrate the effect of the symmetry breaking on the

*kuzmiak@ufe.cz

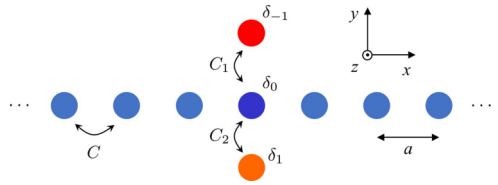

FIG. 1. A coupled-waveguide system consisting of a one-dimensional array and two additional waveguides above and below the array.

reflectance spectra. In Sec. IV we interpret the observed spectral features in terms of the poles and zeros of the scattering matrix by using the Weierstrass factorization theorem. Section V is devoted to the resonance associated with the quasi-BIC mode; we show that the relevant part of the spectrum can be rewritten into the form of the Fano formula.

II. MODEL

We use the standard approach based on the coupled mode theory (CMT) [13–15]. The total field in the structure is expressed through superposition of modal fields in the individual waveguides with slowly varying amplitudes $\psi_m(z)$ ($m \in Z$) on the mth waveguide in the array and $\varphi_{\mp1}(z)$ on the upper and lower additional waveguide. The dependence of fields on time t and the z axis is assumed to be of the form $[\varphi_{-1}(z)\ \psi_m(z)\ \varphi_1(z)]\exp(i\omega t - i\beta z)$, where β is a suitably chosen reference propagation constant. The evolution of the modal amplitudes is described within CMT by a set of coupled equations,

$$i\psi_m' = C(\psi_{m-1} + \psi_{m+1}), \qquad m \neq 0, \tag{1}$$

$$i\psi_0' = \delta_0\psi_0 + C(\psi_{-1} + \psi_1) + C_1\varphi_{-1} + C_2\varphi_1, \tag{2}$$

$$i\varphi_{-1}' = \delta_{-1}\varphi_{-1} + C_1\psi_0, \tag{3}$$

$$i\varphi_1' = \delta_1\varphi_1 + C_2\psi_0, \tag{4}$$

where the prime stands for the derivative with respect to z, C is the coupling coefficient in the array, $C_{1,2}$ are the coupling coefficients between the upper and lower additional waveguide and the 0th waveguide in the array, and δ_0 and $\delta_{\mp1}$ are self-coupling coefficients in the 0th waveguide in the array and in the upper and lower additional waveguides, respectively. The self-coupling coefficients may include the effect of nearest neighbors due to the geometry as well as the possible external perturbations of the 0th waveguide and the additional waveguides. Note that self-coupling coefficients associated with the other waveguides in the array ($m \neq 0$) do not appear explicitly in Eq. (1) due to the periodicity, the coefficients are the same and their effect is implicitly included in the value of the reference propagation constant β [14]. In the following we assume that $\delta_0, \delta_{\mp1} \in R$ and $C, C_{1,2} > 0$.

We seek the stationary solutions of Eqs. (1)–(4) in the form $[\varphi_{-1}(z)\psi_m(z)\varphi_1(z)] \propto \exp(-i\varepsilon z)$, where ε stands for the change in the propagation constant and corresponds to the energy in the quantum theory. The unperturbed array described by Eq. (1) supports propagation of the Bloch waves $\psi_m = A\exp(-ik_x am - i\varepsilon z)$, where k_x is the Bloch wave-number and a is the period of the lattice with the well-known dispersion relation,

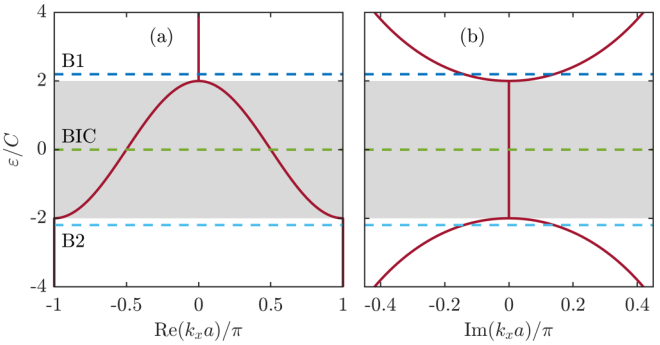

FIG. 2. Solution of the dispersion equation (5) for the periodic array. Solid lines display the dependence of the energy ε on the real and imaginary parts of the Bloch wave-number k_x; the gray area indicates the continuum. The dashed horizontal lines indicate energy levels of the bound states in the composed structure with parameters $C_1 = C_2 = C$ and $\delta_{-1} = \delta_1 = \delta_0 = 0$.

$$\varepsilon = 2C\cos(k_x a), \tag{5}$$

(see, e.g., Ref. [16]). The corresponding band structure including positions of the states in the band gap [i.e., solutions of Eq. (5) with complex k_x] is shown in Fig. 2 and shows that the periodic array supports the continuum of extended states in the band $-2C < \varepsilon < 2C$.

The composed structure exhibits rich modal behavior; the spectrum was classified in Ref. [10], here we summarize the main features and present additional details regarding the numerical procedure. The eigenmodes corresponding to the solutions of Eqs. (1)–(4) are assumed to be in the form

$$\psi_m = Ae^{-ik_x a|m| - i\varepsilon z}, \tag{6}$$

$$\varphi_{\pm1} = B_{\pm1}e^{-i\varepsilon z}. \tag{7}$$

Let us first consider the case when $\varepsilon = \delta_1$ or $\varepsilon = \delta_{-1}$. It follows from Eqs. (1)–(4) that the nonzero solution is not supported unless the structure possesses the vertical symmetry $\delta_{-1} = \delta_1$ when one obtains a bound state,

$$\varepsilon = \delta_{-1} = \delta_1 \tag{8}$$

$$C_1B_{-1} = -C_2B_1, \qquad A = 0. \tag{9}$$

The eigenvalue ε, see Eq. (8), is doubly degenerate, and the eigenfunction is vertically antisymmetric in sense of Eq. (9). The mode is the symmetry-protected BIC provided $-2C < \delta_{\pm1} < 2C$.

Now let us turn to the case when $\varepsilon \neq \delta_1$ and $\varepsilon \neq \delta_{-1}$. We substitute Eqs. (6) and (7) into Eqs. (2)–(4) and after a few steps of algebra obtain the eigenvalue equation,

$$2C\sin(k_x a) + i\mu = 0, \tag{10}$$

where

$$\mu = \delta_0 + \frac{C_1^2}{\varepsilon - \delta_{-1}} + \frac{C_2^2}{\varepsilon - \delta_1}. \tag{11}$$

None of the solutions of Eq. (10) is a true BIC as the derivation assumes $A \neq 0$, however, for the vertically asymmetric structures ($\delta_{-1} \neq \delta_1$), one of them may represent a quasi-BIC as will be shown below.

It is advantageous to rewrite Eq. (10) into the form

$$4C^2 \sin^2(k_x a) = -\mu^2. \tag{12}$$

Now we use Eq. (5) and express the left-hand side of Eq. (12) in terms of the energy ε. The resulting equation can be cast in the form of a sixth-order polynomial in ε, and its roots are equal to mode energies. When applicable, the solution given in Eq. (8) is also included as a double root; however, the root itself is not a solution of Eq. (12). The corresponding wave-numbers $k_x a$ can be determined by solving of Eq. (5), which in general provides 12 solutions (two for each eigenvalue ε) such that $-\pi < \mathrm{Re}(k_x a) \leqslant \pi$, whereas six of them satisfy Eq. (10). As will be discussed in Sec. IV, the solutions $p \equiv k_x a$ of Eq. (10) coincide with the poles of the S-matrix, the remaining six values, $z \equiv k_x a$, coincide with the zeros of the S-matrix. The energy eigenvalues are either real or occur in complex conjugate pairs ε, $\varepsilon' = \varepsilon^*$ with pole pairs p, $p' = -p^*$. This property can be explained as a consequence of the time-reversal symmetry [17]. The modes with complex energies satisfy either outgoing, $0 < \mathrm{Re}(p) \leqslant \pi$ (conventional definition of leaky modes), or ingoing boundary conditions, $-\pi < \mathrm{Re}(p') < 0$, and these conditions manifest themselves in energy eigenvalues as $\mathrm{Im}(\varepsilon) < 0$ and $\mathrm{Im}(\varepsilon') > 0$, respectively. The latter statement follows from Eqs. (5) and (10).

As an example we consider the spectrum of vertically symmetric structures $\delta_{-1} = \delta_1$ that are defined by the parameters $\delta_{\mp 1} = \delta_0 = 0$. In this degenerate case, Eq. (10) yields only four roots, which can be expressed analytically as

$$\varepsilon = \pm\sqrt{2C^2 \pm 2\sqrt{C^4 + C_{\mathrm{av}}^4}}, \tag{13}$$

where all combinations of the signs are allowed and $C_{\mathrm{av}}^2 = (C_1^2 + C_2^2)/2$. The corresponding modes exhibit vertical symmetry,

$$C_2 B_{-1} = C_1 B_1. \tag{14}$$

Consequently, the structures for arbitrary $C_{1,2}$ support three bound modes with real energies, their levels being depicted in Fig. 2 for the case of $C_1 = C_2 = C$. Two of them, denoted as B1 and B2, are given by Eq. (13) and stay localized outside the continuum with the corresponding poles $\mathrm{Re}(k_x a) = 0$ and $\mathrm{Re}(k_x a) = \pi$. The remaining confined mode is a doubly degenerate BIC with zero energy, see Eq. (8), which formally coincides with the poles $k_x a = \pm\pi/2$. In addition, Eq. (13) provides a pair of eigenvalues with pure imaginary energies, the corresponding states are denoted as L, L′ [10], whereas their energy and pole pairs satisfy the symmetries described above.

The structures with broken vertical symmetry, $\delta_1 \neq \delta_{-1}$, cannot support BIC, instead we observe a new mode pair (qBIC, qBIC′) initially with complex energies with one of them being a quasi-BIC leaky mode (qBIC). The full spectrum of modes is shown in Fig. 3, the modes are labeled according to their asymptotics when $\delta_{\pm 1} \to 0$. We note that an arbitrary choice of the structural parameters may lead to a

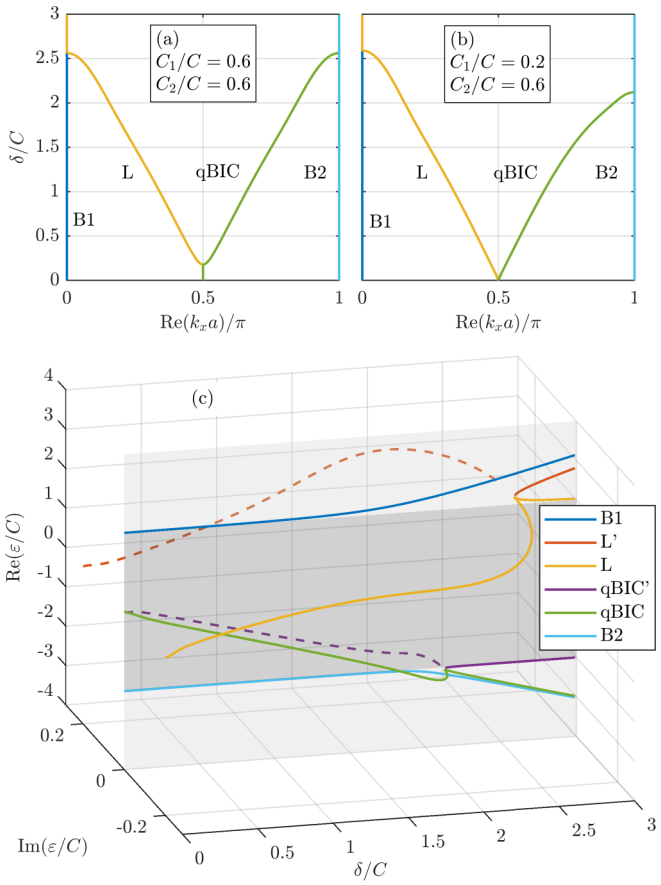

FIG. 3. Modes of structures with broken vertical symmetry $\delta = -\delta_{-1} = \delta_1$. (a) and (b) Dependencies of the asymmetry strength δ on the real part of the Bloch wave-number k_x; (c) the real and imaginary parts of the energy ε vs the asymmetry strength δ, the dashed lines indicate the states with $\mathrm{Im}(\varepsilon) > 0$, and the gray areas indicate the continuum in the plane $\mathrm{Im}(\varepsilon) = 0$. Parameters (a) $C_1 = C_2 = 0.6C$; (b) and (c) $C_1/C = 0.2$, $C_2/C = 0.6$; $\delta_0 = 0$.

complicated behavior. We found that the parameter δ_0 does not affect qualitatively the features associated with the excitation of a quasi-BIC. Moreover, the difference between δ_1 and δ_{-1} rather than actual values of the parameters crucially affects the behavior of the modes. Therefore, in the following, we focus on the structures that are defined as $\delta \equiv \delta_1 = -\delta_{-1}$ and $\delta_0 = 0$ where the strength of the asymmetry between δ_1 and δ_{-1} is expressed in terms of the parameter δ. Figures 3(a) and 3(b) demonstrate behavior of poles $k_x a$ with increasing δ, we display only symmetric part of the spectra $0 \leqslant \mathrm{Re}(k_x a) \leqslant \pi$, i.e., the modes B1, B2, qBIC, and L, the remaining poles for qBIC′ and L′ are placed symmetrically with respect to $\mathrm{Re}(k_x a) = 0$. Figure 3(c) shows behavior of all six complex eigenvalues ε. We observe two bound modes (B1 and B2) with real energies outside the continuum, the related poles have $\mathrm{Re}(k_x a) = 0$ and $\mathrm{Re}(k_x a) = \pi$, and modes L and L′ which now exhibit general complex energy.

Let us first consider the structures with small levels of asymmetry strength δ. Lifting the degeneracy of BIC leads to appearance of the qBIC leaky mode $\mathrm{Im}(\varepsilon) < 0$ and the qBIC′ mode, representing states with $\mathrm{Im}(\varepsilon) > 0$; both the modes become BIC in the limit $\delta \to 0$ where they coalesce [Fig. 3(c)].

The evolution of the corresponding poles starts from their initial positions at $k_x a = \pm\pi/2$ [Figs. 3(a) and 3(b)]. For the structures with identical coupling coefficients, $C_1 = C_2$, the real components $\mathrm{Re}(k_x a)$ of the poles of qBIC, L modes are the same and equal $\pi/2$ until a critical value of parameter δ is achieved [Fig. 3(a)]. Likewise, $\mathrm{Re}(k_x a) = -\pi/2$ applies to the poles of qBIC′ and L′ modes below the same critical value, The critical value corresponds to the first type of the exceptional point (EP) described in Ref. [10].

In the case when $C_1 \neq C_2$ the attraction between qBIC and L modes disappears as well as the EP and instead, the splitting of $\mathrm{Re}(k_x a)$ associated with the (qBIC, L) and (qBIC′, L′) pairs occurs at $\delta = 0$ [Fig. 3(b)]. With increasing δ the modes reach the second type of the EP at which the energies of L, L′, qBIC, and qBIC′ modes become real and correspond to the bound states outside the continuum.

III. TRANSMITTANCE AND REFLECTANCE

To complete the description of the states supported by the structure we also calculated the effect of the additional waveguides on scattering of the Bloch waves propagating in the array. Instead of Eq. (6), the field amplitudes in the array are now expressed through the amplitude transmittance t and reflectance r as

$$\psi_m = e^{-ik_x am - i\varepsilon z} + re^{ik_x am - i\varepsilon z}, \quad m \leqslant 0, \tag{15}$$

$$\psi_m = te^{-ik_x am - i\varepsilon z}, \quad m \geqslant 0. \tag{16}$$

whereas Eq. (7) for amplitudes in the additional waveguides reamins valid. After substituting Eqs. (7), (15), and (16) into Eqs. (2)–(4) one obtains

$$(\delta_{-1} - \varepsilon)B_{-1} + C_1 t = 0 \tag{17}$$

$$(\delta_1 - \varepsilon)B_1 + C_2 t = 0, \tag{18}$$

and the final result,

$$t = r + 1 = \frac{2C\,\sin(k_x a)}{2C\,\sin(k_x a) + i\mu}, \tag{19}$$

according to which the solutions of the dispersion equation (10) are linked to the poles of t and r.

To demonstrate elementary properties of Eq. (19) we present in Fig. 4 reflectance spectra $R = |r|^2$ for vertically symmetric, $\delta_{\mp 1} = 0$, (dashed line) and asymmetric, $\delta_{-1} \neq \delta_1$, (solid line) structures.

(1) The reflectance reaches maximum $R = 1$ at the continuum band edges due to vanishing group velocity. Indeed, according to Eq. (19) $\sin(k_x a) = 0$ when $k_x a = 0$ or $k_x a = \pm\pi$.

(2) To interpret the other peaks $R = 1$ in the continuum, we consider isolated additional waveguides. Each of them supports one localized state possessing $\varepsilon = \delta_{\pm 1}$. For the composed structure, the transmission vanishes at these energies due to the vanishing denominators in the second or third term in Eq. (11) and, thus, $|\mu| \to \infty$ in Eq. (19). According to Eqs. (17) and (18) we, in general, observe two different resonances: (i) $\varepsilon = \delta_{-1}$ with $B_{-1} \neq 0$ and $B_1 = 0$ and (ii) $\varepsilon = \delta_1$ with $B_1 \neq 0$ and $B_{-1} = 0$. In other words, for asymmetric structures and $|\delta| < 2C$ we always observe two peaks

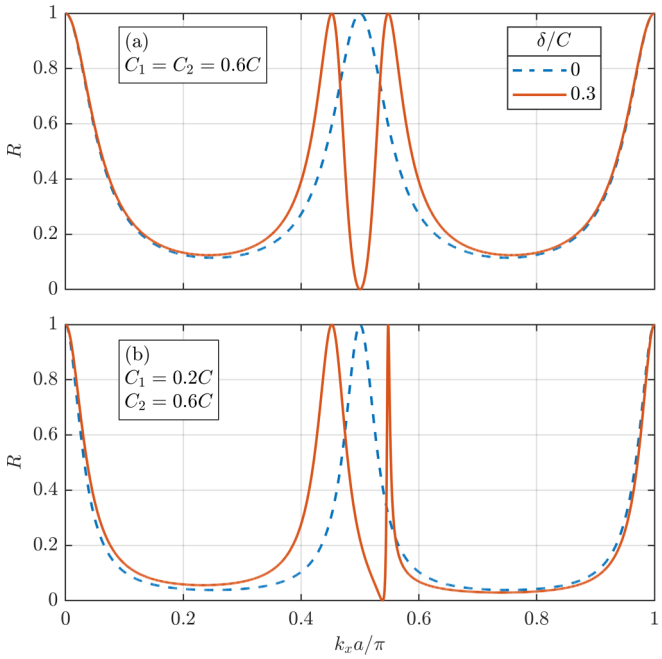

FIG. 4. The reflectance R vs the Bloch wave-number k_x; dashed line: system with the symmetry $\delta = 0$; solid line: system with the broken symmetry $\delta/C = 0.3$. The coupling coefficients C_1 and C_2 are indicated in the boxes $\delta_0 = 0$.

at $k_x a = \arccos[\delta_{\mp 1}/(2C)]$. At each resonance, the field in one of the attached waveguides is *not* excited as demonstrated in Fig. 5 (see solid lines only), whereas for symmetric structures [Fig. 5 (dashed lines)], the two resonances coalesce into single one with both additional waveguides being excited.

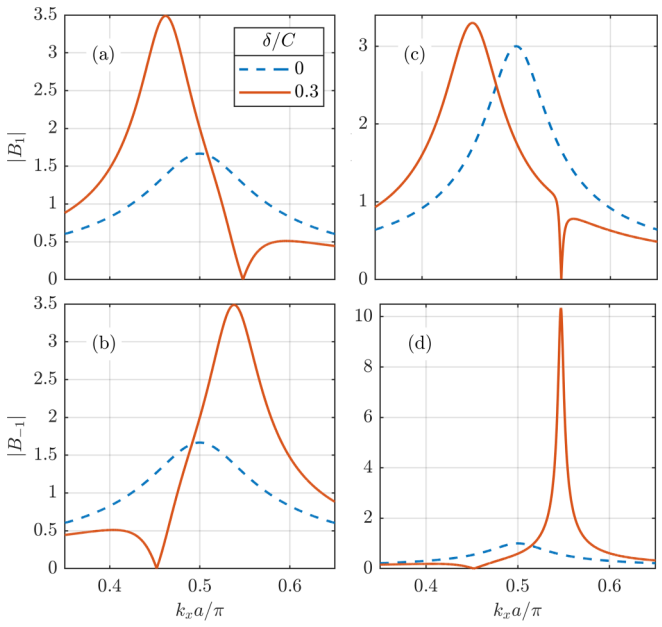

FIG. 5. Field amplitudes $B_{\pm 1}$ for the parameters in Fig. 4: (a) and (b) $C_1 = C_2 = 0.6C$; (c) and (d) $C_1 = 0.2C$, $C_1 = 0.6C$; dashed lines: system with the symmetry $\delta = 0$; solid lines: system with the broken symmetry $\delta/C = 0.3$.

(3) The positions of the peaks $R = 1$ do not depend on the coupling coefficients $C_{1,2}$. On the other hand, $C_{1,2}$ have profound influence on the shape of the resonances: decreasing of C_1/C and C_2/C (weaker coupling) leads to narrower peaks in R, whereas asymmetry in $C_{1,2}$ strongly affects asymmetric behavior of the two resonances for $\delta > 0$, cf. Figs. 4(a) and 4(b); Figs. 5(a)–5(d). Moreover, the position of global minima $R = 0$ which occurs at $\delta > 0$, strongly depends on both asymmetries, in $C_{1,2}$ and $\delta_{\mp 1}$ with the corresponding energy for $\delta_0 = 0$ given by the relation,

$$\varepsilon = \frac{C_1^2 - C_2^2}{C_1^2 + C_2^2}\delta. \tag{20}$$

In the next section we show that the described features can be interpreted in terms of excitation of various modes of the system.

It is worth noting that Eq. (20) describes also approximately the real part of the energy eigenvalue $\mathrm{Re}(\varepsilon)$ for qBIC, which captures the behavior of qBIC for small δ in Figs. 3(a) and 3(b) as well as with Figs. 5(a) and 5(c) in Ref. [10]. For the imaginary part of the eigenvalue we obtained

$$\mathrm{Im}(\varepsilon) \approx -\frac{8C_1^2C_2^2}{\left(C_1^2 + C_2^2\right)^3}\delta^2. \tag{21}$$

Both results follow from the perturbation analysis of Eqs. (1)–(4). Equation (21) predicts that the decay rate, which is proportional to $-\mathrm{Im}(\varepsilon)$, increases quadratically with the asymmetry strength δ. This is in accord with the behavior of qBIC observed in Figs. 5(b) and 5(d) in Ref. [10] as well as nicely agrees with the trend observed in Fig. 4 in Ref. [12].

IV. MODAL EXPANSION OF SCATTERING SPECTRA

We start with the S-matrix that for our structure has the form

$$\hat{S} = \begin{pmatrix} r & t \\ t & r \end{pmatrix}. \tag{22}$$

Eigenvectors of $\hat{S}$ have even and odd symmetries [17] with corresponding eigenvalues $S_e = r + t$ and $S_o = r - t$. In comparison with Ref. [17], we do not reverse the sign of S_o. Conversely, if we know the eigenvalues, we can determine the reflection and transmission coefficients as

$$r = \frac{S_e + S_o}{2}, \quad t = \frac{S_e - S_o}{2}. \tag{23}$$

It follows from Eq. (19) that for our structure $S_o = -1$ and

$$S_e = \frac{2C\,\sin(k_x a) - i\mu}{2C\,\sin(k_x a) + i\mu}. \tag{24}$$

The dependence $S_e(q)$, $q \equiv k_x a$, can be expressed using the Weierstrass factorization theorem [17,18] as

$$S_e(q) = Ae^{iBq}\prod_n \frac{q - z_n}{q - p_n}, \tag{25}$$

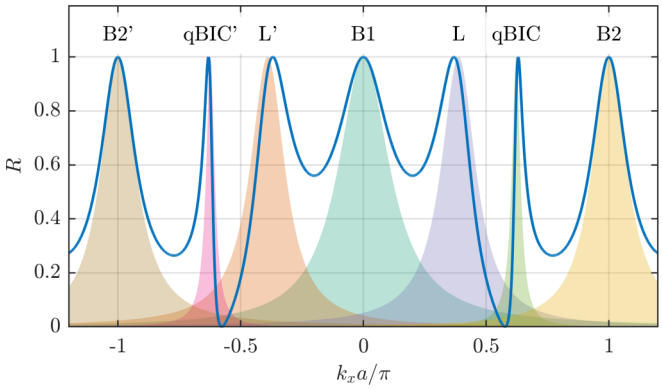

FIG. 6. The reflectance R vs the Bloch wave-number k_x (solid line) for the system with the parameters $C_1 = 0.5C$, $C_2 = C$, $\delta = -\delta_{-1} = \delta_1 = 0.8C$, and $\delta_0 = 0$. The shaded areas present contributions of various modes in the expansion given by Eq. (25).

where z_n and p_n are zeros and poles of $S_e(q)$ and

$$A = S_e(0)\prod_n \frac{p_n}{z_n}, \tag{26}$$

$$iB = \frac{S_e'(0)}{S_e(0)} + \sum_n \left(\frac{1}{z_n} - \frac{1}{p_n}\right). \tag{27}$$

The time-reversal symmetry of the physical systems requires that the number of poles and zeros should be equal [17,18], and this property was used in the formulation of Eq. (25). It follows from Eq. (24) that the poles p_n correspond to modes of the structure, cf. Eq. (10), whereas the zeros z_n correspond to solutions of Eq. (10) in which the sign of the term $i\mu$ is the opposite. Thus, both poles and zeros can be found simultaneously by solving Eq. (12). For each pole p_n there is a zero p_n^* which yields the relation $z_n = p_n^*$. The knowledge of the pole-zero pairs is sufficient to restore the diagonal component of the scattering matrix $S_e(q)$ through Eq. (25) and the spectra r and t through Eq. (23).

To evaluate the contributions of various modes to the scattering spectra we repeat the same procedure with a single selected mode (pole-zero pair) used in the expansion given by Eq. (25). The results are demonstrated in Fig. 6. To enhance visibility of the main features we choose an asymmetric structure such as in Fig. 4(b) (solid line) with increased values of δ and $C_{1,2}$ that lead to a significant overlap among various peaks. Figure 6 displays the reflectance R as a function of the Bloch wave-number k_x; the extended range of k_x was chosen with the aim to present the effect of the resonances with $\mathrm{Re}(p_n)$ outside of the physical interval $0 \leqslant k_x a \leqslant \pi$. The solid curve displayed is calculated by using the exact formula given by Eq. (19), however, the same dependence is obtained by using Eqs. (25) and (23) provided that a sufficient number of the pole-zero pairs is taken into account; here we used all pairs fulfilling the condition $-6\pi < \mathrm{Re}(p_n) \leqslant 6\pi$. This relatively wide range of $\mathrm{Re}(p_n)$ is consistent with our definition of the structural parameters. For structures exhibiting narrower peaks (such as in Fig. 4) the required range of $\mathrm{Re}(p_n)$ can be considerably reduced.

The evaluation of the A and B deserves an additional comment: It can be shown that by using Eqs. (26) and (27) one

obtains $|A| = 1$ and $B \in R$. A and B depend on the number of pole-zero pairs used in the expansion (25), therefore, the dependence $S_e(q)$ comforms to the values $S_e(0)$ and $S'_e(0)$ in Eqs. (26) and (27). However, the evaluation requires the knowledge of universal values of A and B which are independent of the $S_e(0)$, $S'_e(0)$ and of the number of pole-zero pairs. To determine such values we consider the structure which does not support any resonance, i.e., q is far from each resonance and has vanishing reflectance $r = 0$. No resonance implies absence of the pole and, therefore, Eq. (25) yields $S_e(q) = A\exp(iBq)$. Consequently, one obtains $A = 1$ and $B = 0$. This result was numerically verified.

The shaded areas in Fig. 6 present the contributions of various modes in the expansion given by Eq. (25) to the total spectra. The individual peaks have Lorentzian profile and the total spectrum appears as a result of their interference [17,18]. Obviously, all spectral features correspond to the individual modes: B1 and B2 are responsible for peaks at band edges whereas L and qBIC for the peaks in the continuum. We note that even the modes L′ and qBIC′ may affect the spectra (in particular, the values of R in proximity of the local minima) in the physical range of $0 \leqslant k_x a \leqslant \pi$, provided the overlap is sufficiently large. As the most interesting feature appears to be the destructive interference mainly between L and qBIC modes (or L′ and qBIC′) leading to global minima $R = 0$.

V. FANO RESONANCE

Figure 6 indicates that the asymmetric Fano shape associated with the qBIC mode arises due to the superposition of modes L and qBIC. In this section we confirm this statement by direct calculation. First, we will describe a part of spectrum near an arbitrary resonance defined with a selected pole-zero pair p_s, $z_s = p_s^*$, and later we choose a specific case of the qBIC mode. Likewise in Ref. [17], we rewrite Eq. (25) into the form

$$S_e(q) = e^{i\varphi(q)}\frac{q - p_s^*}{q - p_s}, \tag{28}$$

where the phase $\varphi(q)$ describes the effect of other modes on the spectrum. The selected resonance corresponds to the discrete state in the Fano theory whereas $\varphi(q)$ can be regarded as the slowly varying phase shift of the continuum. Next, we introduce the normalized "frequency" detuning,

$$\Omega = \frac{q - \mathrm{Re}(p_s)}{\mathrm{Im}(p_s)}, \tag{29}$$

and calculate the reflectance $R = |r|^2$. We substitute Eq. (28) into Eq. (23) where we also use $S_o = -1$ to obtain

$$R = \frac{1}{2}\mathrm{Re}\left[1 - e^{i\varphi}\frac{\Omega + i}{\Omega - i}\right] = \frac{[\Omega\,\sin(\varphi/2) + \cos(\varphi/2)]^2}{\Omega^2 + 1}. \tag{30}$$

The last expression leads to the following formula:

$$R = \left(\frac{1}{1 + f^2}\right)\frac{(\Omega + f)^2}{\Omega^2 + 1}, \tag{31}$$

which is identical with the famous relation for the Fano resonance [6] in the form that is normalized to maximum 1—see the prefactor $1/(1 + f^2)$ and where the Fano parameter f reads as

$$f = \cot(\varphi/2). \tag{32}$$

The Fano formula on the right-hand side of Eq. (31) applies also for the transmittance $T = 1 - R$ provided we change the Fano parameter as $f \to -1/f$.

The result can be further simplified when we assume that the continuum is formed only by one resonance with pole p_c, and the related phase shift φ is assumed to be constant within the range of the selected narrow resonance q_s, $\varphi(q) \approx \varphi[\mathrm{Re}(q_s)]$. Under these assumptions, it follows from

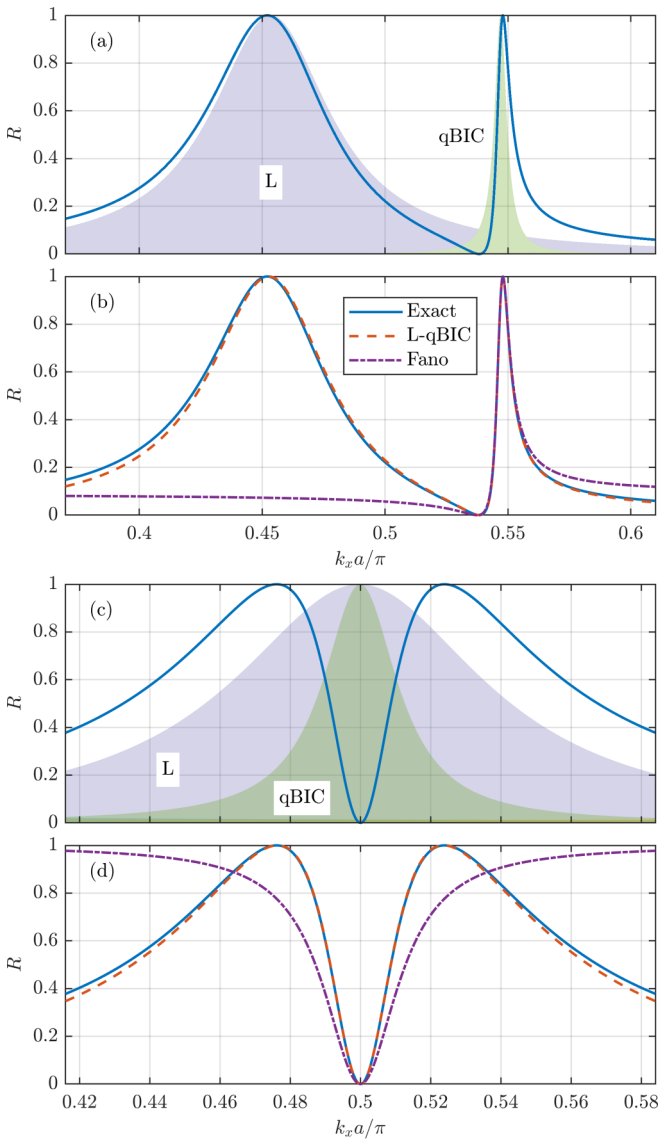

FIG. 7. The reflectance R vs the Bloch wave-number k_x. Parameters (a) and (b) $C_1/C = 0.2$, $C_2/C = 0.6$, $\delta/C = 0.3$. (c) and (d) $C_1 = C_2 = 0.6C$, $\delta/C = 0.15$. $\delta_0 = 0$. "Exact" (solid lines) in (a)–(d): exact calculation through Eq. (19). The shaded areas in (a) and (c): individual contributions of L and qBIC modes in Eq. (25). "'L-qBIC'" (dashed lines) in (b) and (d): L and qBIC modes used in Eq. (25) simultaneously. Fano (dashed-dot lines) in (b) and (d): Fano formula Eq. (31).

comparison of Eqs. (28) and (25) that

$$e^{i\varphi} \approx \frac{\mathrm{Re}(p_s) - p_c^*}{\mathrm{Re}(p_s) - p_c}. \tag{33}$$

Consequently, we obtain from Eq. (32),

$$f \approx \frac{\mathrm{Re}(p_s) - \mathrm{Re}(p_c)}{\mathrm{Im}(p_c)}. \tag{34}$$

Figure 7 demonstrates the effect of the L mode on the spectra near the qBIC mode, therefore, we choose in the calculation p_s as the qBIC mode and p_c as the L mode. At first, we consider structures with $C_1 \neq C_2$: Fig. 7(a) shows the contributions of the interacting modes L and qBIC to the total spectra, whereas Fig. 7(b) shows that for the selected structural parameters, it is sufficient to take into account only the interaction of the L and the qBIC modes. The effect of all other modes is marginal—see the curves labeled as Exact and L-qBIC. Furthermore, we observe that the Fano formula Eq. (31) for which Eq. (34) provides $f = 3.2$ describes quite well the asymmetric shape of the spectra near the chosen qBIC resonance $k_x a \sim 0.55$, whereas outside this region, the description is not valid as our assumption $f = \text{const}$ is not satisfied.

Similar behavior was observed in structures with $C_1 = C_2$: In Fig. 7(c) the contributions of the interacting modes L and qBIC to the total spectra are depicted. The former ones appear at the same positions of $\mathrm{Re}(k_x a) = \pi/2$ due to the selected asymmetry strength δ below its branching value—see also Fig. 3(a). Figure 7(d) demonstrates that it is sufficient to take into account only the interaction of L and qBIC modes and that the resulting dip in R arises due their destructive interference—see the curves labeled as Exact and L-qBIC. We note that Eq. (34) provides $f = 0$, consequently, the Fano formula Eq. (31) describes a symmetric dip, its shape agrees reasonably well with the reference profile only in the close proximity of the resonance.

VI. CONCLUSION

In conclusion, we studied systematically spectral and scattering properties of a photonic analog of an extended Fano-Anderson tight-binding model. The complex eigenvalues reveal interesting phenomena, such as exceptional points and level repulsion, and offer an interesting alternative where the $\mathcal{PT}$-symmetry phase transition occurs without gain and loss. We establish the conditions under which the structure supports the symmetry-protected BIC. In the case of the broken vertical symmetry the BIC couples to the continuum, turns into the quasi-BIC leaky mode, and manifests itself as a generally asymmetric Fano resonance in the scattering spectra. The key spectral features can be interpreted in terms of system eigenmodes through a generalized Weierstrass factorization theorem. In particular, we found that the Fano resonance arises from the interference between two leaky modes, one of them being the quasi-BIC. The reflectance (or transmittance) can be rewritten into the form of the Fano formula where the shape parameter f can be expressed in terms of the poles belonging to the quasi-BIC and the other leaky mode. Our paper provides the theoretical framework which describes transformation of the symmetry-protected BIC into a leaky mode and allows to interpret the resonant properties of the more complex systems, whereas through the engineering of zeros of the transmission matrix, it enables to investigate their nontrivial topological properties and may prove to be useful in various fields of optics as well as in cold matter and quantum confined systems.

ACKNOWLEDGMENT

We acknowledge financial support by the Czech Science Foundation (CSF) through Project No. 1900062S.

[1] J. von Neumann and E. Wigner, Phys. Z. **30**, 465 (1929).
[2] C. W. Hsu, B. Zhen, A. D. Stone, J. D. Joannopoulos, and M. Soljačić, Nat. Rev. Mater. **1**, 16048 (2016).
[3] S. I. Azzam and A. V. Kildishev, Adv. Optical Mater. **9**, 2001469 (2021).
[4] K. Koshelev, A. Bogdanov, and Y. Kivshar, Opt. Photonics News **31**, 38 (2020).
[5] A. Krasnok, D. Baranov, H. Li, M.-A. Miri, F. Monticone, and A. Alu, Adv. Opt. Photon. **11**, 892 (2019).
[6] U. Fano, Phys. Rev. **124**, 1866 (1961).
[7] G. D. Mahan, *Many-Particle Physics* (Kluwer Academic/Plenum, New York, 2000), p. 44; p. 208.
[8] A. E. Miroshnichenko, S. F. Mingaleev, S. Flach, and Y. S. Kivshar, Phys. Rev. E **71**, 036626 (2005).
[9] S. Weimann, Y. Xu, R. Keil, A. E. Miroshnichenko, A. Tünnermann, S. Nolte, A. A. Sukhorukov, A. Szameit, and Y. S. Kivshar, Phys. Rev. Lett. **111**, 240403 (2013).
[10] J. Petráček and V. Kuzmiak, arXiv:2205.03775.
[11] B. P. Nguyen, K. Kim, F. Rotermund, and H. Lim, Phys. Status Solidi B **249**, 1765 (2012).
[12] Y. Plotnik, O. Peleg, F. Dreisow, M. Heinrich, S. Nolte, A. Szameit, and M. Segev, Phys. Rev. Lett. **107**, 183901 (2011).
[13] A. Hardy and W. Streifer, J. Light. Technol. **3**, 1135 (1985).
[14] F. Ye, D. Mihalache, B. Hu, and N. C. Panoiu, Phys. Rev. Lett. **104**, 106802 (2010).
[15] X. Shi, X. Chen, B. A. Malomed, N. C. Panoiu, and F. Ye, Phys. Rev. B **89**, 195428 (2014).
[16] T. Pertsch, T. Zentgraf, U. Peschel, A. Bräuer, and F. Lederer, Appl. Phys. Lett. **80**, 3247 (2002).
[17] V. Grigoriev, S. Varault, G. Boudarham, B. Stout, J. Wenger, and N. Bonod, Phys. Rev. A **88**, 063805 (2013).
[18] V. Grigoriev, A. Tahri, S. Varault, B. Rolly, B. Stout, J. Wenger, and N. Bonod, Phys. Rev. A **88**, 011803(R) (2013).

Correction: A missing sign in a relation in the fifth sentence of the fifth paragraph in Sec. II has been corrected. A typographical error in the penultimate sentence of the seventh paragraph in Sec. II has been corrected.